

Disrupting Adversarial Transferability in Deep Neural Networks

Christopher Wiedeman, Ge Wang

Rensselaer Polytechnic Institute

Abstract

Adversarial attack transferability is a well-recognized phenomenon in deep learning. Prior work has partially explained transferability by recognizing common adversarial subspaces and correlations between decision boundaries, but we have found little explanation in the literature beyond this. In this paper, we propose that transferability between seemingly different models is due to a high linear correlation between features that different deep neural networks extract. In other words, two models trained on the same task that are seemingly distant in the parameter space likely extract features in the same fashion, just with trivial shifts and rotations between the latent spaces. Furthermore, we show how applying a feature correlation loss, which decorrelates the extracted features in a latent space, can drastically reduce the transferability of adversarial attacks between models, suggesting that the models complete tasks in semantically different ways. Finally, we propose a Dual Neck Autoencoder (DNA), which leverages this feature correlation loss to create two meaningfully different encodings of input information with reduced transferability.

1. Introduction

1.1 Background

The advancement of artificial intelligence, especially deep learning (DL), has revolutionized research in computer vision, natural language processing, and recently many other fields, including medical image reconstruction. Unfortunately, the development of adversarial attacks against deep learning models has highlighted a glaring lack of robustness in DL methods. Adversarial attacks to deep neural networks were first discussed in 2014 when Szegedy, et al. showed that adding deliberately crafted but imperceptible perturbations to MNIST digit images would cause a trained classifier to catastrophically misclassify the sample [1]. Since then, successful adversarial attacks have been demonstrated in numerous other DL contexts, such as speech-to-text translation and medical image reconstruction [2], [3]. Counterintuitively, networks that can generalize to never-seen natural samples cannot perform well on samples very close to previously seen samples. Such a discovery not only raises security concerns but also questions whether DL models truly learn the desired features for a given task.

Initially, it was thought that adversarial samples were a product of overfitting, and partially due to the capacity for deep neural networks to fit overly-complex decision boundaries, but lower capacity networks and less complex machine learning models are actually more vulnerable to adversarial attacks [4]–[6]. On the contrary, the current thinking is that data-driven models (particularly more linear models) only learn samples along a data manifold within the input space, whereas adversarial examples exist off-manifold. Complex, highly non-linear networks with

sufficient training data are required to expand this manifold, which becomes increasingly challenging in high-dimensional input spaces.

An intriguing property of adversarial attacks is their transferability between models, i.e., adversarial samples trained to target one model are often successful against other models, even when these models are trained with different data or use different architectures [1]. This phenomenon has been well-observed, and carries implications for black-box attacks, where an attacker does not have access to the target model.

While previous work has confirmed adversarial transferability and even rationalized their existence by showing correlations in decision boundaries, it is not understood why these correlations exist in DL models with vastly different parameters. In this paper, we first observe that although DL models may be distant in the parametric space and produce different hidden states, the extracted information is likely identical in essence. More specifically, for a set of samples, the hidden state extracted using one model can easily be correlated with the hidden state from another model with a simple affine transformation. Furthermore, we demonstrate that breaking this correlation leads to much lower transferability between adversarial samples.

1.2 Preliminaries

For a comprehensive review on the research in adversarial attacks, we recommend reading *Adversarial Attacks and Defenses in Deep Learning* by Ren, et al. [7].

Types of attacks: An untargeted adversarial attack is one that does not seek a specific result (e.g., misclassification into a specific class) aside from maximally degrading a performance measure of the model. If f is a trained model, with a loss objective $J(\theta, x, y)$ where θ are the model parameters and $\{x, y\}$ are data inputs and labels respectively, then an untargeted attack based on sample/label pair $\{x_i, y_i\}$ finds point x_i' near x_i that maximizes the loss:

$$x_i' = \underset{x_i'}{\operatorname{argmax}} J(\theta, x_i', y_i), \quad D(x_i, x_i') \leq \epsilon \quad (1)$$

where D is some distance metric. In the following work, we use the norm $L_\infty(x_i - x_i')$ for D , as this is the most used distance metric in adversarial attacks, although L_0 , L_1 , and L_2 are also occasionally used. Numerous methods have been discovered to find adversarial attacks, many of which rely on first-order optimization. In this work, we will primarily focus on two common search methods: Fast Gradient Sign Method (FGSM) [5] and Projected Gradient Descent [6], [8]. FGSM is favored for its simplicity and efficiency:

$$x' = x + \epsilon \operatorname{sgn}(\nabla_x J(\theta, x, y)) \quad (2)$$

On the other hand, PGD is like FGSM, but uses a random initialization and iteration to find stronger attacks. Clipping is used to keep the sample within the distance constraint and data range:

$$x^{t+1} = \operatorname{Clip}(x^t + \alpha \operatorname{sgn}(\nabla_x J(\theta, x, y))) \quad (3)$$

where α is some step size. PGD is considered a strong attack, and attaining robustness against this method will generally defend against other attacks [6].

Adversarial attacks are referred to as either white, gray, or black box attacks to specify the attacker’s knowledge on the target model. In white box attacks, the attacker has full access to the model’s architecture and parameters. In gray box attacks, the attacker only knows the model architecture, and black box attackers assume no information on the target model. In both gray and black box scenarios, an attacker typically trains a surrogate model as the target model, and then crafts attacks using this surrogate. While white box attacks are understandably the most potent, gray and black box attacks have been also shown potency due to high attack transferability between models.

Related Work: To our best knowledge, Szegedy et al. raised the first concern regarding adversarial stability of DNNs in 2014 [1]. A plethora of work proposing both new attack and defense methods has been published since then. Carlini and Wagner have contributed much research to stronger attack methods, including the creation of C&W attacks that are effective against many earlier defenses such as defensive distillation [9]–[11]. Papernot, et al. also proposed a class of algorithms that use an adversarial saliency map to produce targeted (i.e., producing a specific result) attacks [12]. A few works also used generative adversarial networks to produce attacks [13], [14].

On the defense side, it is crucial to distinguish between adversarial defenses and true adversarial robustness. Many adversarial defenses achieve success against specific, often weaker attacks, but seemingly fail against stronger attacks. It was discovered that many of these methods defend against unsophisticated attacks because they obfuscate the loss gradient, making effective attacks harder to find [15]. In this sense, the network is secure against weak attacks but not truly robust, since adversarial examples still exist, and can be exploited with stronger algorithms. Currently, the only approach that has demonstrated true robustness is adversarial training, in which a network is trained with adversarial examples. Numerous methods, including GAN-based adversarial sample generation have been explored [5], [6], [14], [16]. Robustness against strong attacks, however, requires training on strong examples, which are prohibitively expensive in most contexts, and high-capacity networks for fitting complex decision boundaries [6].

Transferability: The transferability of adversarial samples--a major concern for black-box security threats--is not fully understood. Numerous works have recognized attack transferability (especially among smaller models), and some rationalize their existence either by pointing out that many points of high loss/instability exist in these models, or that decision boundaries of samples are correlated between different models. To the first point, it was shown that DNNs are often robust to random perturbations (e.g., Gaussian noise) while still being highly vulnerable to adversarial attacks [1]. This suggests that while many adversarial examples may exist, the total adversarial space is not random and still small relative to the high dimensional input space; the intersection of these spaces between models cannot be attributed to mere coincidence. To the second explanation, there is indeed strong evidence that the decision boundaries around samples are correlated between different models, and that adversarial samples exist in subspaces that often intersect [17]. This phenomenon is clearly observed in *universal adversarial perturbations*, which generalize not only between models, but also between different input samples due to strong correlations between decision boundaries [18], [19]. Still, this explanation does not explain *why* these decision

boundaries and subspaces are correlated between models with entirely different parameters or architectures.

In this paper, we unpeel one more layer of the transferability puzzle by first demonstrating that DNNs trained on the same task are actually quite similar in the way they complete tasks, regardless of how different the models are in the parameter space. In fact, we find that the features that two models extract are semantically identical, and with one simply being an affine-transformed version of the other. More importantly, we show that breaking this correlation drastically reduces the transferability of adversarial samples between models. Finally, we illustrate this concept of breaking transferability with a dual-neck autoencoder (DNA), which creates two unique input encodings (also referred to as bottlenecks) with a limited number of layers added to a traditional autoencoder.

2. Transferability and Feature Correlation between Models

When adversarial attacks were first discovered, the natural method was to train an ensemble of models that would only reach a consensus on benign samples. Surely, networks with different parameters would resolve a task in different ways and diverge on adversarial samples. As discussed above, however, transferability dictates that these networks not only fail on the same adversarial samples, but also fail in the same way (i.e., reach similar incorrect outputs). As such, the question remains: why do different networks behave nearly identically at unstable inputs, and how does one train meaningfully different models?

A naïve approach to this question would be to maximize the distance between two models in the parameter space, as it is known that DNNs typically do not converge to a global minimum, but rather approach one of many local minima that perform well. This method understandably assumes that differently parameterized models solve a task in different ways. To test this, we designed a simple CNN for MNIST classification and trained two models f_1 and f_2 in parallel (architecture in Appendix). To incentivize parametric distance, we added a loss term to encourage a desired Frobenius norm D_t (set to 1000, 1500, 2000, 2500, and 3000 in different trials) between the parameters θ_1 and θ_2 :

$$J(\theta_1, \theta_2, x, y) = \text{CE}(f_1(\theta_1, x), y) + \text{CE}(f_2(\theta_2, x), y) + \lambda(D_t - \|\theta_1 - \theta_2\|_2^2)^2 \quad (4)$$

with CE as the cross-entropy function between logits and labels. After training a pair of networks, we computed FGSM attacks of varying magnitude ϵ for one network and tested their transferability to the other network (Figure 1). We found that transferability unsurprisingly increased with attack magnitude, but there was no correlation at all between transferability and distance in the parameter space, contradicting the notion that parametrically distant networks solve tasks in different ways.

To investigate this further, we analyzed one of the late hidden states (Appendix 7.1) of inputs to model pairs. If $X \in \mathbb{R}^{N \times D}$ is a batch of N input samples, then $Z_1, Z_2 \in \mathbb{R}^{N \times M}$ are vectorized hidden features of length M from the two models respectively. We found that Z_1 and Z_2 were accurately relatable by a simple linear regression:

$$Z_2 = Z_1 W ; Z_1 = [Z_1, 1] \quad (5)$$

where the matrix W contains the optimal regression weights using ordinary least squares. More specifically, we measured the Pearson correlation coefficient for various batches of X and found it to be < 0.975 on average.

$$R^2 = 1 - \frac{SS_{res}}{SS_{total}} = 1 - \frac{\left\| \left(I - (\mathbf{Z}_1^\top \mathbf{Z}_1)^{-1} \mathbf{Z}_1^\top \right) \mathbf{Z}_2 \right\|_2^2}{\|\mathbf{Z}_2\|_2^2} \quad (6)$$

This high degree of correlation not only held for natural samples, but also for adversarial samples, and was true regardless of the parametric distance between the two models (Figure 1), revealing a strong, consistent linear relationship between the two encodings. This finding is in line with observations from [1], [20], which note that individual units in latent spaces do not correspond to useful information; rather, vectors in the space as a whole represent features. Similarly, the latent features extracted by two separate models in this instance are numerically different but encode the same semantic information. Furthermore, the relationship between the two encodings is linear, with one being an affine transformation of the other. This also suggests that DNNs distant in the parametric space are not necessarily semantically different; rather, they can (and often do) encode the same information, only differing by trivial transformations in their latent spaces (e.g., rotations, expansions/contractions, shifts). This insight helps explain why optimizing for a global minimum is not necessary, and why numerous local minima with similar loss values exist in the parameter space, as these points do not represent semantically different models. It is no wonder that these ‘different’ neural networks perform similarly on adversarial examples.

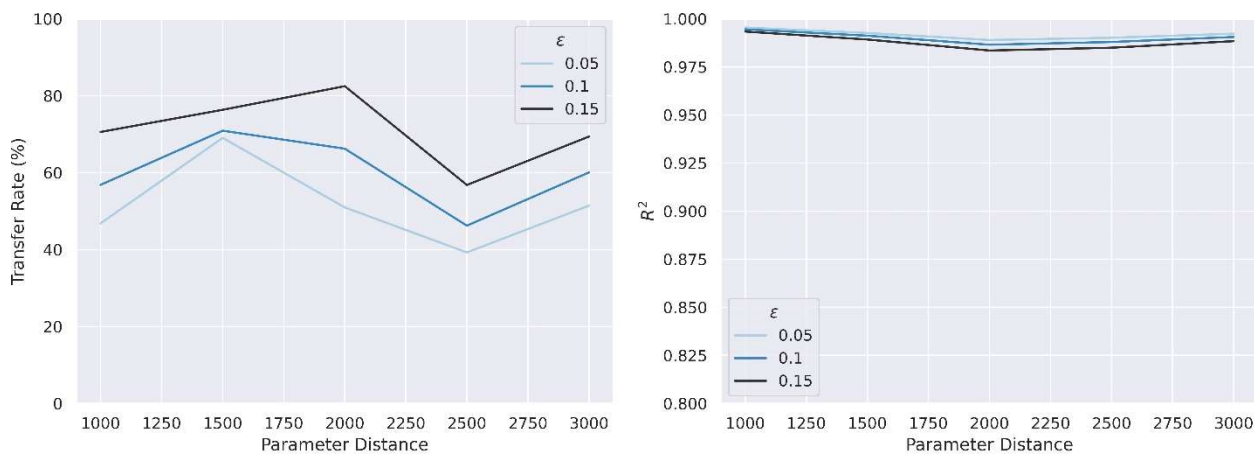


Figure 1: Semantically same encoding with different distances in the space of network parameters. (Right): Attack transferability rate vs parametric distance between network pairs. Transferability is measured as the proportion of adversarial attacks from one model that successfully cause misclassification on the opposing network. Parameter distance is measured as the square Frobenius norm $\|\theta_1 - \theta_2\|_2^2$. (Left): Correlation coefficient between vectorized latent features extracted from either model while processing adversarial samples. ϵ is the FGSM attack magnitude.

3. Disrupting Transferability through Decorrelating Features

Given such a linear correlation between features extracted by networks, a natural question is how networks would behave if this correlation is disrupted. We test this scenario by once again

training two classifying CNNs in parallel, but introduce a decorrelating term \mathcal{L}_R to decouple the latent features extracted by the two models:

$$J(\theta_1, \theta_2, x, y) = \text{CE}(f_1(\theta_1, x), y) + \text{CE}(f_2(\theta_2, x), y) + \lambda \mathcal{L}_R(f_1, f_2, \theta_1, \theta_2, x) \quad (7)$$

This decorrelating term, which is also referred to as correlation loss, is essentially the correlation coefficient of features Z_1, Z_2 at a proper hidden layer in the neural networks. It was found that using the log transform and inserting a small constant value ε (set to 0.001 in all of our experiments) is beneficial for stability:

$$\begin{aligned} \mathcal{L}_R &= \log(SS_{total} + \varepsilon) - \log(SS_{res} + \varepsilon) \\ \mathcal{L}_R &= \log(\|Z_2\|_2^2 + \varepsilon) - \log\left(\left\| \left(I - (Z_1^\top Z_1)^{-1} Z_1^\top \right) Z_2 \right\|_2^2 + \varepsilon\right) \end{aligned} \quad (8)$$

Practically speaking, Z_1 is usually not full column rank. While solutions exist for theoretically more stable rank-deficient pseudo-inverse computations, we found that the most practical method is to first use a QR decomposition to find dependent columns of Z_1 and remove them. Algorithm 1 summarizes this process.

Algorithm 1
<i>#N: batch size</i>
<i>#Z₁, Z₂ ∈ ℝ^{N×M}: vectorized batch features from two networks</i>
<i>#ε = 0.001: constant for stability</i>
<i>#η = 0.0005: criteria for determining independent columns</i>
<i>_, R = QR(Z₁) #QR decomposition</i>
<i>column_index = abs(diag(R))/max(diag(R)) > η #find index of independent columns</i>
<i>Z₁ = [Z₁[:, column_index], 1] #remove dependent columns and augment in 1s column</i>
<i>SS_{res} = ‖(I - (Z₁[⊤]Z₁)⁻¹Z₁[⊤])Z₂‖₂² #Residual sum of squares from the OLS solution</i>
<i>SS_{total} = ‖Z₂‖₂² #Total sum of squares</i>
<i>ℒ_R = log(SS_{total} + ε) - log(SS_{res} + ε)</i>

Figure 2 compares the transferability of the trained CNN pairs with and without use of the correlation loss. We found that weighting \mathcal{L}_{corr} ($\lambda = 0.05$) led to a significant reduction in adversarial transferability over all tested magnitudes ($\varepsilon = 0.05, 0.10, 0.15$), although stronger attacks are unsurprisingly still associated with greater transferability. Furthermore, imposing this constraint had minimal effects on natural sample, which only reduced from 97% to 94.875% on average.

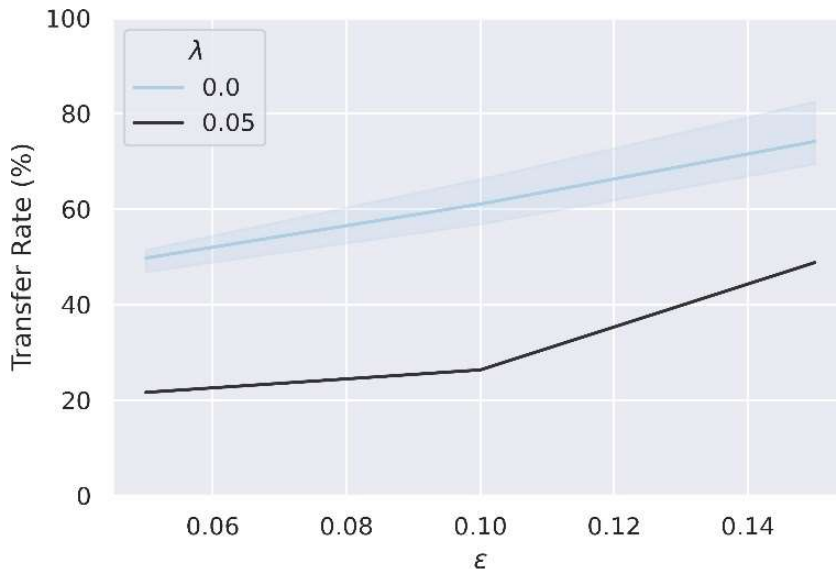


Figure 2: Transfer rates of adversarial attacks between a CNN pair using the regularization by Eq. (8) ($\lambda = 0.05$) compared with pairs that are only parametrically different ($\lambda = 0.0$). Adversarial attacks were found using FGSM.

4. Dual-Neck Autoencoder (DNA)

4.1 Key idea

To further explore the effect of the correlation loss in training parallel models, we propose a Dual Neck Autoencoder (DNA), which consists of a traditional autoencoder/decoder structure that diverges into two paths at the most compressed hidden layer (i.e., the bottleneck). The most basic motivating concept behind this idea, commonly found in nature and communication systems, is information redundancy: two differently processed but overlapping information representations are encoded and decoded in parallel. The majority of the architecture must be shared between encoding pathways (otherwise, the aggregate will essentially be two entirely separate models), yet the pathways must be meaningfully different, lest both pathways will only contain trivial differences (spatial rotations, shifts, etc.) and will suffer from identical instabilities.

Figure 3 illustrates the general structure of our proposed DNA. A shared encoder block first processes and partially compresses the input. This encoding is then fed into two bottleneck modules, each of which further compresses the information before partially decompressing. During training, the latent representations at the most compressed state are compared between the two bottlenecks using the correlation loss. The two partial decompressions are then both fully decompressed with a common decoder, producing two separate reconstructions. In the experiments, a trained classifier is also stacked at the end of this module to evaluate the reconstructions.

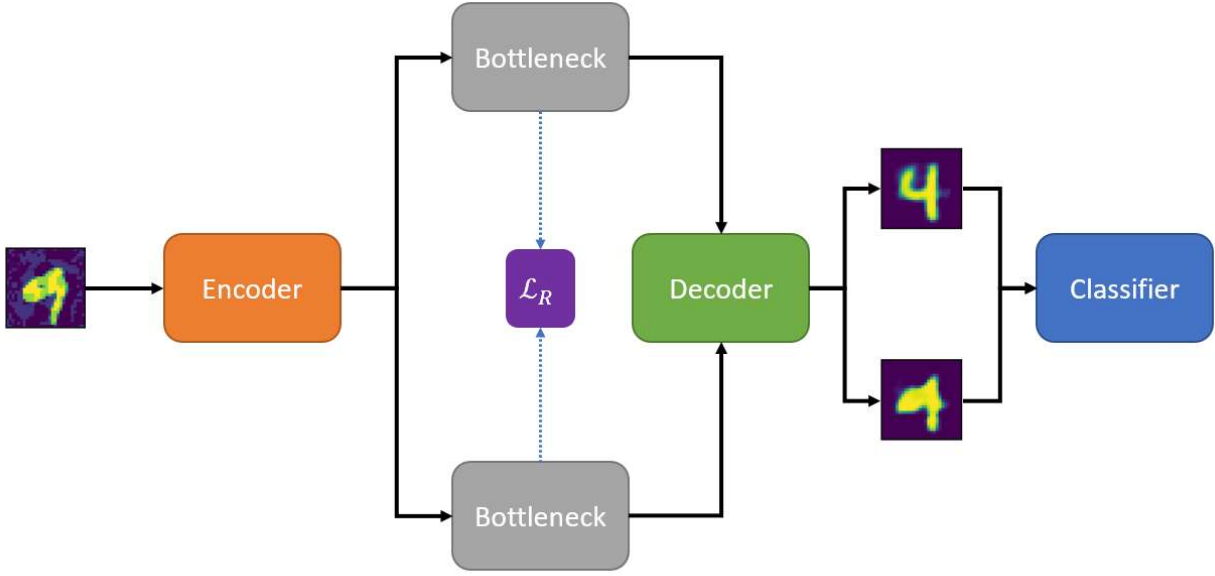


Figure 3: Proposed dual neck autoencoder (DNA). A common encoder and decoder are shared to compress and decompress information respectively. Two separate bottleneck modules differently encode information into fully compressed states which are decorrelated using the correlation loss term. The decoder produces a separate reconstruction from each encoding.

4.2 Methods

Both the MNIST Digit and CIFAR-10 datasets were used to test DNA. Simple fully connected architectures for MNIST and convolutional architectures for CIFAR-10 were designed for the encoder, bottleneck, and decoder blocks shown in Figure 3. Exact architectures are illustrated in Appendix 7.2. In both cases, the DNA was first trained for reconstruction fidelity with the following loss function:

$$J_{DNA}(F, Z, x_i) = \text{MSE}(F(x_i, \theta)_1, x_i)^2 + \text{MSE}(F(x_i, \theta)_2, x_i)^2 + \lambda \mathcal{L}_R(F, \theta, x_i) \quad (9)$$

where MSE is the mean-square error between two arguments, $F(\cdot)_n$ is the n_{th} reconstruction pathway (e.g., $encoder \rightarrow bottleneck_n \rightarrow decoder$), x_i is an input batch of images, and $\theta = [\theta_{encoder}, \theta_{bottleneck}, \theta_{bottleneck2}, \theta_{decoder}]$ are the network parameters. $\mathcal{L}_R(F, \theta, x_i)$ uses the compressed bottleneck representations for correlation comparison (see Appendix 7.2). Note that if one disregards the correlation loss, this is the squared L_2 norm of the mean-square errors of the two reconstructions, which is preferred to avoid a ‘sparse’ solution (i.e., avoid the optimizer only improving one reconstruction at the expense of the other).

Part of our goal in testing the DNA is to generate adversarial attacks and observe if the divergent structure and decorrelation mechanism can break transferability between the two reconstructions. Attacks targeting the mean square error of either reconstruction simply results in added background noise in the output rather than differences in semantic content (e.g., causing the autoencoder to reconstruct a perceptually different digit). As such, we attach a classifier C after the DNA and attack pathway n and define the cross-entropy objective:

$$J(F, C, x_i) = \text{CE}(C(F(x_i, \theta)_n), y_i) \quad (10)$$

For each dataset, we run two trials using $\lambda = 0$ (no correlation loss) and $\lambda = 0.05$. For each trial, we first briefly trained a DNA using the loss in Eq. (9) and then a separate classifier to classify the output images (15 epochs each for MNIST, 30 epochs for CIFAR-10). After this, we targeted the model using adversarial attacks of magnitude $\epsilon = 0.05, 0.1, 0.15$ for MNIST and $\epsilon = 2/255, 4/255, \text{ and } 8/255$ for CIFAR-10 while recording classification accuracies using the classifier with either DNA output. Each of the two reconstruction pathways were separately attacked using the objective in Eq. (10), and recorded accuracy metrics are the average result of these attacks.

As previously mentioned, adversarial training is the most successful recorded method in increasing robustness, but is prohibitively expensive using strong attacks (e.g., PGD). Training with weaker, more accessible FGSM attacks acts positively as a regularizer but will not add defense against stronger attacks. Still, we also tested how DNA could benefit from this regularization by briefly training it to reconstruct natural inputs from $\epsilon = 0.1$ FGSM samples (classifier module is not adversarial trained).

All models were implemented using Pytorch 1.8.1 on an Nvidia Titan RTX GPU with 24GB of VRAM.

4.3 Results

All of the following results are in the context of classification accuracy. Four distinct metrics are presented for evaluating the DNA reconstruction:

- `dual_correct`: Proportion of test data in which *both* reconstructions are classified correctly.
- `either_correct`: Proportion of test data in which *only one* reconstruction is classified correctly. This metric is expected to be low when attacks are highly transferable.
- `dual_incorrect`: Proportion of test data in which *both* reconstruction is classified *incorrectly*.
- `det_correct`: Proportion of test data in which the reconstruction more coherent with the input (i.e., lower mean-square error) is correctly classified. This is used as a simple criteria for selecting the ‘superior’ reconstruction.

4.3.1 MNIST

Figure 4 illustrates classification metrics for DNA reconstructions of MNIST digit data under PGD attacks. Unsurprisingly, all reconstruction accuracies under decreased with higher magnitude attacks. It is also noteworthy that the higher fidelity reconstruction accuracy (‘`det_correct`’) for $\lambda = 0.05$ is superior to that of $\lambda = 0.0$ on adversarial samples, and this difference increased with attack magnitude. The ‘`either_correct`’ metric is also nearly zero for $\lambda = 0.0$ for all attacks. Figure 5 and Figure 6 respectively report accuracy metrics for PGD and FGSM attacks respectively after weak adversarial training of the DNA, both reflect similar comparative trends. They also indicate a benefit from brief, weak adversarial training, as classification accuracies on all reconstruction models/pathways were improved.

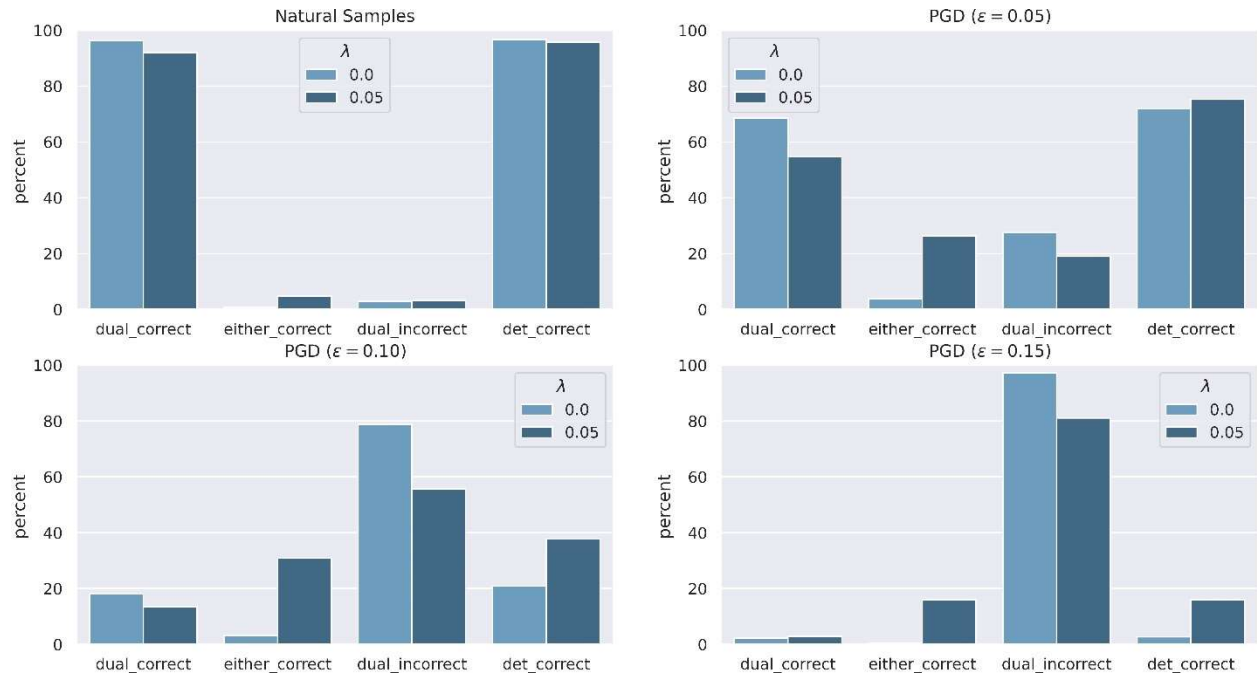


Figure 4: Accuracy metrics of DNA with the CNN classifier on MNIST dataset with PGD attacks of varying magnitude ϵ . All graphs compare DNAs with ($\lambda = 0.05$) and without ($\lambda = 0.0$) bottleneck decorrelation. The four metrics are as follows: *dual_correct*: both reconstructions from DNA are classified correctly; *either_correct*: only one of the reconstructions is classified correctly; *dual_incorrect*: both reconstructions are incorrectly classified; *det_correct*: the reconstruction closer to the original input (lower mean-square error) is classified correctly.

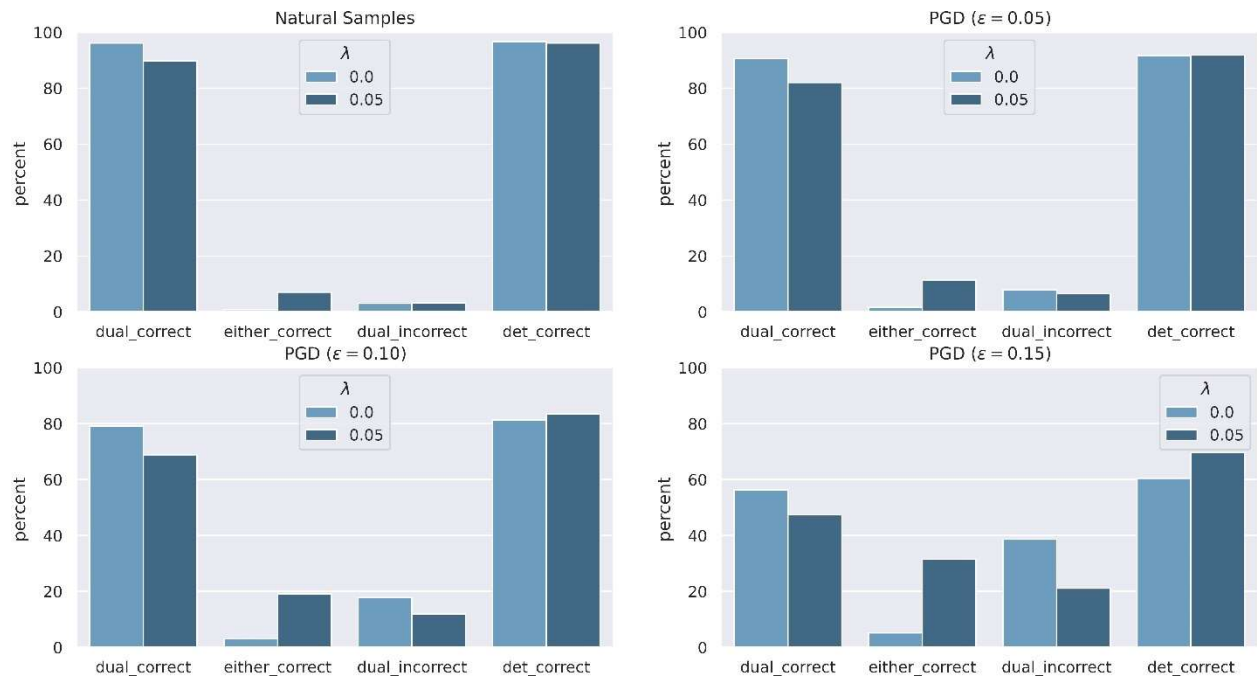


Figure 5: Accuracy metrics of DNA after weak (FGSM) adversarial training with the CNN classifier on the MNIST dataset with PGD attacks of varying magnitude ϵ . All graphs compare DNAs with ($\lambda = 0.05$) and without ($\lambda = 0.0$) bottleneck decorrelation. The four metrics are the same as defined in Figure 4.

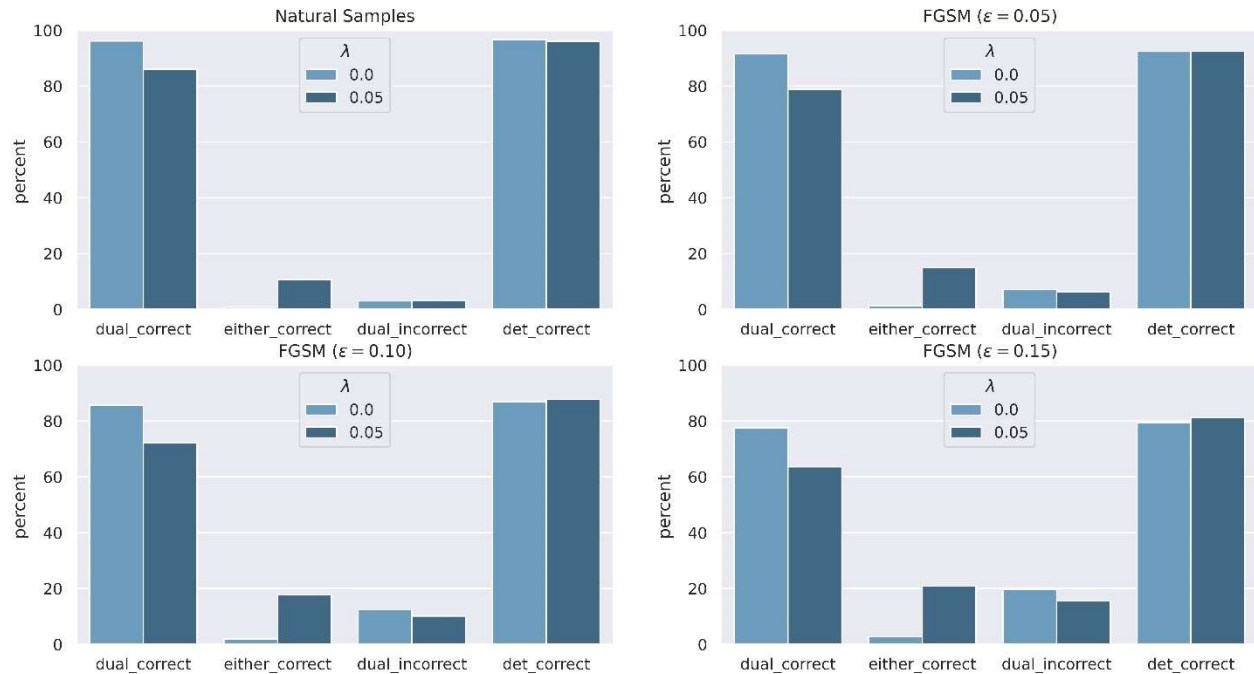


Figure 6: Accuracy metrics of DNA after weak (FGSM) adversarial training with the CNN classifier on the MNIST dataset with FGSM attacks of varying magnitude ϵ . All graphs compare DNAs with ($\lambda = 0.05$) and without ($\lambda = 0.0$) bottleneck decorrelation. The four metrics are the same as defined in Figure 4.

Additionally, Figure 7 shows five examples of digit reconstructions from adversarial examples. Qualitatively, one can see that the attack causes a semantic corruption in one of the bottleneck encodings, but this corruption does not transfer to the alternative bottleneck, despite sharing the same encoder/decoder layers.

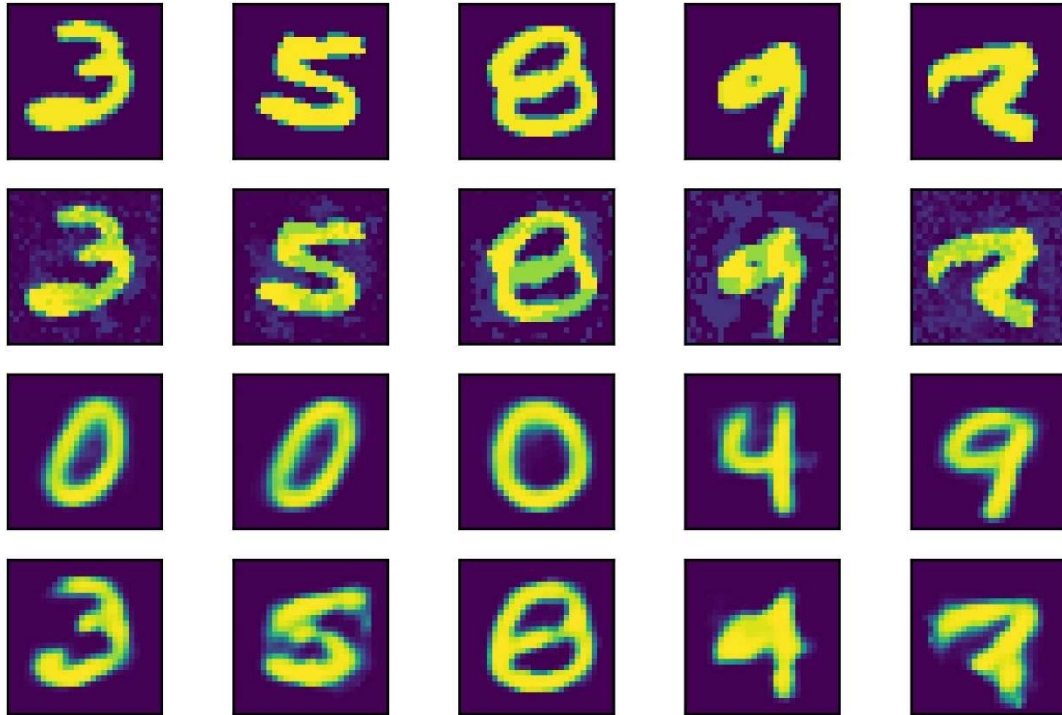


Figure 7: Example reconstructions of classification-based strong adversarial (PGD, $\epsilon = 0.15$) attacks from DNA. 1st row: Natural samples. 2nd row: Perturbed samples. 3rd row: Reconstructions from one targeted bottleneck. 4th row: Reconstructions from the other bottleneck.

4.3.2 CIFAR-10

Figure 8 and Figure 9 illustrate accuracy metrics for FGSM and PGD attacks respectively for the CIFAR-10 DNA reconstructions. Classification accuracies are overall lower than the results seen in MNIST experiments, but the overall trends are similar, and the ‘either_correct’ metric is minimal in all cases for $\lambda = 0.0$.

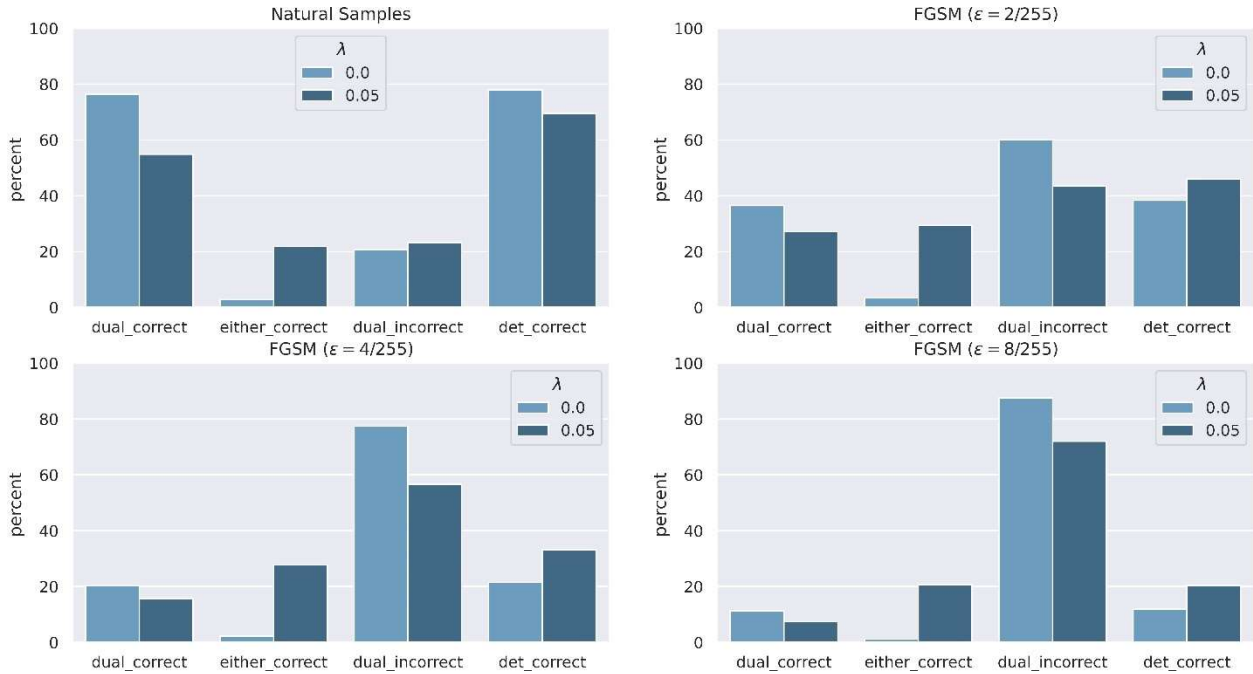


Figure 8: Accuracy metrics of DNA with the CNN classifier on the CIFAR-10 dataset with FGSM attacks of varying magnitude ϵ . All graphs compare DNAs with ($\lambda = 0.05$) and without ($\lambda = 0.0$) bottleneck decorrelation.

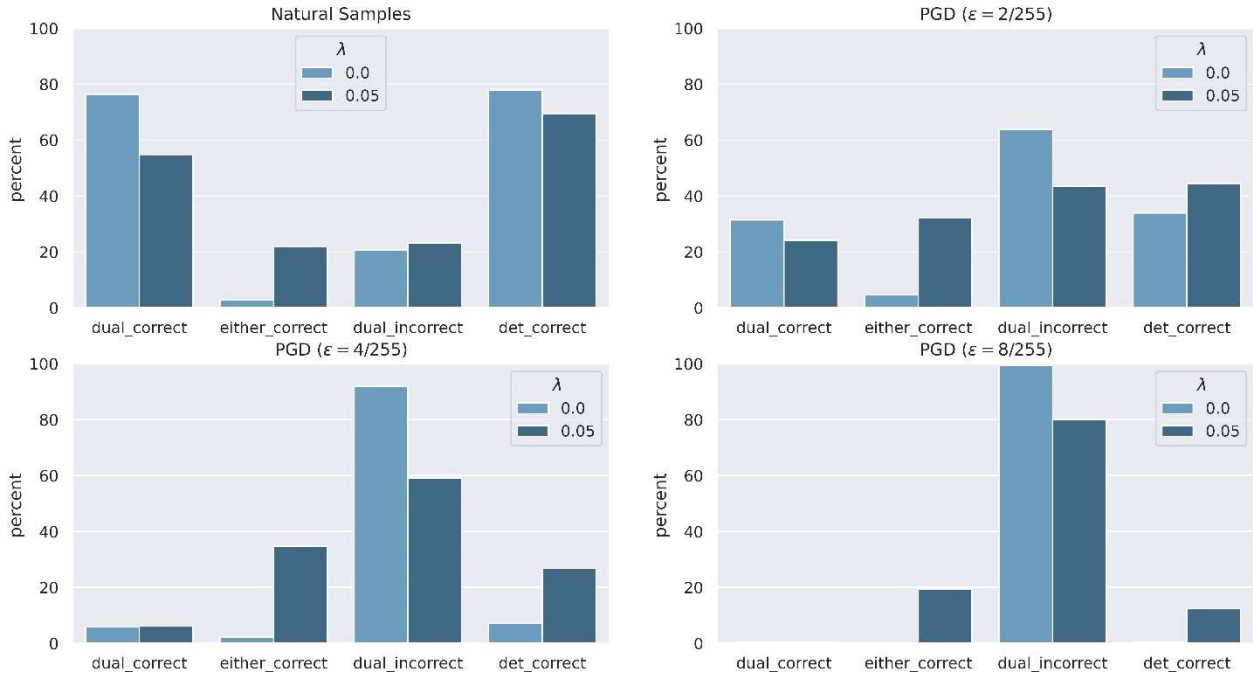


Figure 9: Accuracy metrics of DNA with the CNN classifier on the CIFAR-10 dataset with PGD attacks of varying magnitude ϵ . All graphs compare DNAs with ($\lambda = 0.05$) and without ($\lambda = 0.0$) bottleneck decorrelation.

5. Discussions

Overall, results both from the parallel classifier and DNA experiments indicate that imposing the proposed feature correlation loss between two models or pathways reduces the transferability of adversarial attacks. In particular, the DNA architecture demonstrated reduced transferability

even when most of the encoder/decoder model were shared. This is clearly seen in Figures Figure 4, Figure 5, Figure 6, Figure 8, and Figure 9, where the ‘either_correct’ metric is nearly zero for all $\lambda = 0.0$ models (indicating perfect transferability) but substantial for $\lambda = 0.05$. Although transferability still increases with attack magnitude in all the cases, the relative benefit having meaningfully different reconstruction pathways increases, as evidenced by the increasing accuracy difference of ‘det_correct’ between $\lambda = 0.0$ and $\lambda = 0.05$.

The results from the DNA experiments also suggest a small tradeoff between reconstruction accuracy on natural samples and decorrelation between reconstruction pathways. In Figures Figure 4, Figure 5, Figure 6, Figure 8, and Figure 9, the ‘dual_correct’ and ‘det_correct’ metrics are consistently higher for $\lambda = 0.0$. Additionally, we found that weighting the correlation loss very heavily $\lambda > 0.1$ greatly decreased overall accuracy. Without any correlation constraint, most likely the model converges both pathways to the same ‘optimal encoding’, whereas imposing this constraint forces the two pathways to compete and compromise for the most meaningful information. It is unclear whether the break in transferability is simply because there is no linear correlation between the feature information, or because there is less mutual information altogether between the two. If linear decorrelation is enough to decrease transferability, then deepening the architecture could mitigate this compromise, as the two bottlenecks could theoretically hold the same information, but with a non-linear relationship. If it is due to less mutual information, however, then this compromise is inherent, since compressing the same input while minimizing mutual information are directly competing tasks.

While the above experiments demonstrate the effect of latent feature correlation, they do not demonstrate state-of-the-art performance by themselves. Numerous limiting factors exist, such as the architectures of both the autoencoder and classifiers, which are easier to train, less complex, and do not leverage various data augmentation and regularization techniques when compared to the state-of-the-art. For comparison, the classifier architectures alone achieved 96% on MNIST and 84% on CIFAR-10 datasets, revealing a small loss in information during compression. In general, results were less desirable on the CIFAR-10 dataset, which is harder to compress due to less similarity among images and higher dimensionality, which increases the adversarial space. It is also possible that in some attack instances, the autoencoder produced a faithful reconstruction with a small perturbation that instead destabilized the classifier. Generally, however, we observed that adversarial perturbations manifested their effect during the autoencoding process.

The computational cost of implementing correlation loss in training is also worth considering on more complex problems, as it requires both QR decomposition and pseudo-inverse computation, both of which are achieved with singular value decomposition (SVD) in most deep learning toolboxes. It also requires a sufficient batch size to ensure that the linear regression is not under-constrained. These factors could be limiting, especially when considering higher dimensional and more varied inputs.

Additionally, while this method shows how one can decrease transferability of adversarial attacks found using common first-order methods, it does not guarantee adversarial robustness. Clearly, each model, and many of these attacks (particularly those with higher magnitude) still

transfer. The results would suggest, however, that linearly decorrelating the latent features at some point in the models will decrease intersection of adversarial subspaces.

The concept of linear feature correlation between models explored here further explains why adversarial attacks transfer, and how seemingly different models could be extracting the same features. In general, this finding is synergistic with other observations of DNNs, including the existence of multiple equivalent local minima in the parameter space during optimization, and naturally diminished attack transferability in sensible high capacity, highly non-linear models, where deep latent spaces may naturally be non-linearly related, but have weaker linear correlation [4], [6]. It would also imply that transferability would be less between models that inherently extract different features due to their architecture: for example CNNs, which focus more on spatially local features, and vision transformers [21], which have larger receptive fields. While transferability between these two architectures has not been investigated to our knowledge, Paul and Chen show very different adversarial noise patterns between vision transformers and CNNs, with transformer perturbations being more distributed in the frequency domain [22].

Practically speaking, the concept of correlational loss could be leveraged in a black-box or grey box setting, where one could first traditionally train a surrogate model, and then also train a true, deployable model for the same task but impose a feature correlation loss between the fixed surrogate and the deployment model, presuming that most black box attacks be optimized to a model like the surrogate. It may also be possible to detect adversarial attacks with an ensemble of networks trained with a correlation loss, since it is less likely that these models would reach a consensus on adversarial samples.

Although the current study has not been focused on any specific task, our idea and findings open a new direction to stabilize deep neural networks. Correlation loss can be further explored to determine whether linear correlation or mutual information as a whole is related to transferability. Much more sophisticated architectures can be designed and evaluated. Hopefully, this line of research will promote accurate and stable real-world AI applications.

6. Conclusion

In this paper, we have demonstrated how adversarial transferability is related to a strong correlation between the features extracted from different models. We have also introduced a novel approach of directly decorrelating these features to reduce attack transferability and demonstrate how even a small pathway deviation along with this decorrelation can reduce transferability of separate reconstructions with a Dual Neck Autoencoder. There are numerous opportunities for further investigations; for example, optimizing this approach and scaling it to larger problems.

7. References

- [1] C. Szegedy *et al.*, “Intriguing properties of neural networks,” *ArXiv13126199 Cs*, Feb. 2014, Accessed: Jun. 30, 2021. [Online]. Available: <http://arxiv.org/abs/1312.6199>

- [2] N. Carlini and D. Wagner, “Audio Adversarial Examples: Targeted Attacks on Speech-to-Text,” *ArXiv180101944 Cs*, Mar. 2018, Accessed: Aug. 12, 2021. [Online]. Available: <http://arxiv.org/abs/1801.01944>
- [3] V. Antun, F. Renna, C. Poon, B. Adcock, and A. C. Hansen, “On instabilities of deep learning in image reconstruction and the potential costs of AI,” *Proc. Natl. Acad. Sci.*, vol. 117, no. 48, pp. 30088–30095, Dec. 2020, doi: 10.1073/pnas.1907377117.
- [4] N. Papernot, P. McDaniel, and I. Goodfellow, “Transferability in Machine Learning: from Phenomena to Black-Box Attacks using Adversarial Samples,” *ArXiv160507277 Cs*, May 2016, Accessed: May 25, 2021. [Online]. Available: <http://arxiv.org/abs/1605.07277>
- [5] I. J. Goodfellow, J. Shlens, and C. Szegedy, “Explaining and Harnessing Adversarial Examples,” *ArXiv14126572 Cs Stat*, Mar. 2015, Accessed: May 20, 2021. [Online]. Available: <http://arxiv.org/abs/1412.6572>
- [6] A. Ma, A. Makelov, L. Schmidt, D. Tsipras, and A. Vladu, “Towards Deep Learning Models Resistant to Adversarial Attacks,” p. 28.
- [7] K. Ren, T. Zheng, Z. Qin, and X. Liu, “Adversarial Attacks and Defenses in Deep Learning,” *Engineering*, vol. 6, no. 3, pp. 346–360, Mar. 2020, doi: 10.1016/j.eng.2019.12.012.
- [8] A. Kurakin, I. Goodfellow, and S. Bengio, “Adversarial examples in the physical world,” *ArXiv160702533 Cs Stat*, Feb. 2017, Accessed: Aug. 12, 2021. [Online]. Available: <http://arxiv.org/abs/1607.02533>
- [9] N. Carlini and D. Wagner, “Defensive Distillation is Not Robust to Adversarial Examples,” *ArXiv160704311 Cs*, Jul. 2016, Accessed: Aug. 13, 2021. [Online]. Available: <http://arxiv.org/abs/1607.04311>
- [10] N. Papernot, P. McDaniel, X. Wu, S. Jha, and A. Swami, “Distillation as a Defense to Adversarial Perturbations against Deep Neural Networks,” *ArXiv151104508 Cs Stat*, Mar. 2016, Accessed: Jun. 10, 2021. [Online]. Available: <http://arxiv.org/abs/1511.04508>
- [11] N. Carlini and D. Wagner, “Towards Evaluating the Robustness of Neural Networks,” *ArXiv160804644 Cs*, Mar. 2017, Accessed: Aug. 12, 2021. [Online]. Available: <http://arxiv.org/abs/1608.04644>
- [12] N. Papernot, P. McDaniel, S. Jha, M. Fredrikson, Z. B. Celik, and A. Swami, “The Limitations of Deep Learning in Adversarial Settings,” *ArXiv151107528 Cs Stat*, Nov. 2015, Accessed: Aug. 13, 2021. [Online]. Available: <http://arxiv.org/abs/1511.07528>
- [13] Y. Song, R. Shu, N. Kushman, and S. Ermon, “Constructing Unrestricted Adversarial Examples with Generative Models,” *ArXiv180507894 Cs Stat*, Dec. 2018, Accessed: Aug. 13, 2021. [Online]. Available: <http://arxiv.org/abs/1805.07894>
- [14] H. Lee, S. Han, and J. Lee, “Generative Adversarial Trainer: Defense to Adversarial Perturbations with GAN,” *ArXiv170503387 Cs Stat*, May 2017, Accessed: Jul. 07, 2021. [Online]. Available: <http://arxiv.org/abs/1705.03387>
- [15] A. Athalye, N. Carlini, and D. Wagner, “Obfuscated Gradients Give a False Sense of Security: Circumventing Defenses to Adversarial Examples,” *ArXiv180200420 Cs*, Jul. 2018, Accessed: May 20, 2021. [Online]. Available: <http://arxiv.org/abs/1802.00420>
- [16] X. Liu and C.-J. Hsieh, “Rob-GAN: Generator, Discriminator, and Adversarial Attacker,” *ArXiv180710454 Cs Stat*, Apr. 2019, Accessed: Jul. 07, 2021. [Online]. Available: <http://arxiv.org/abs/1807.10454>
- [17] F. Tramèr, N. Papernot, I. Goodfellow, D. Boneh, and P. McDaniel, “The Space of Transferable Adversarial Examples,” *ArXiv170403453 Cs Stat*, May 2017, Accessed: Aug. 11, 2021. [Online]. Available: <http://arxiv.org/abs/1704.03453>

- [18] S.-M. Moosavi-Dezfooli, A. Fawzi, O. Fawzi, and P. Frossard, “Universal adversarial perturbations,” *ArXiv161008401 Cs Stat*, Mar. 2017, Accessed: May 20, 2021. [Online]. Available: <http://arxiv.org/abs/1610.08401>
- [19] H. Hirano, A. Minagi, and K. Takemoto, “Universal adversarial attacks on deep neural networks for medical image classification,” *BMC Med. Imaging*, vol. 21, no. 1, p. 9, Jan. 2021, doi: 10.1186/s12880-020-00530-y.
- [20] T. Mikolov, K. Chen, G. Corrado, and J. Dean, “Efficient Estimation of Word Representations in Vector Space,” *ArXiv13013781 Cs*, Sep. 2013, Accessed: Aug. 16, 2021. [Online]. Available: <http://arxiv.org/abs/1301.3781>
- [21] A. Dosovitskiy *et al.*, “An Image is Worth 16x16 Words: Transformers for Image Recognition at Scale,” *ArXiv201011929 Cs*, Jun. 2021, Accessed: Aug. 20, 2021. [Online]. Available: <http://arxiv.org/abs/2010.11929>
- [22] S. Paul and P.-Y. Chen, “Vision Transformers are Robust Learners,” *ArXiv210507581 Cs*, May 2021, Accessed: May 20, 2021. [Online]. Available: <http://arxiv.org/abs/2105.07581>

8. Appendix

8.1 Classifier Architecture used in Section 2

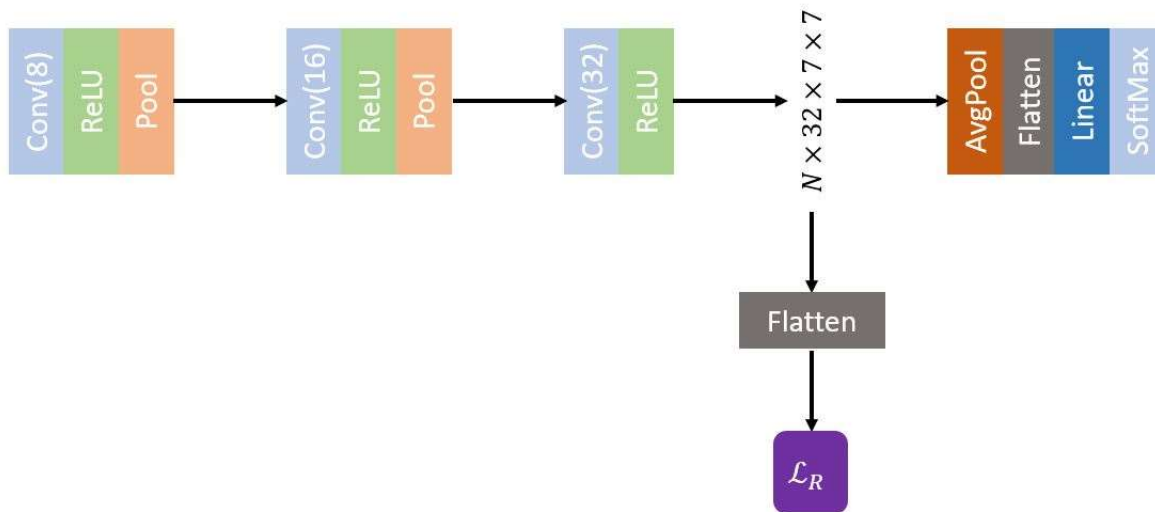


Figure 10: Architecture of the classifier model used to test correlation loss \mathcal{L}_R . Conv(K): 3×3 , 1-stride, zero-padded 2D convolutional layer with K output filters. Pool: 2×2 max pooling. AvgPool: 7×7 average feature pooling. Linear: Densely connected layer with size 10 output. Note that two models of the same architecture were trained in parallel, simultaneously inputting flattened features to \mathcal{L}_R .

8.2 Network Architectures used in Section 3

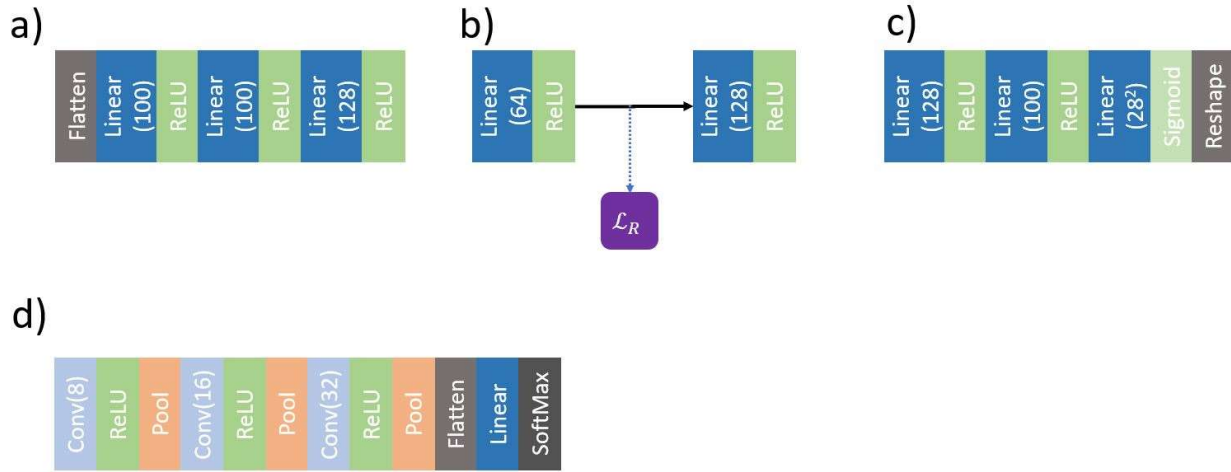


Figure 11: Architectures of a) encoder, b) bottleneck, c) decoder, and d) classifier used in the DNA experiments with the MNIST digit dataset. Conv(K): 3x3, 1-stride, zero-padded 2D convolutional layer with K output filters. Pool: 2x2 max pooling. Linear(K): Densely connected layer with size K (10 if not specified) output.

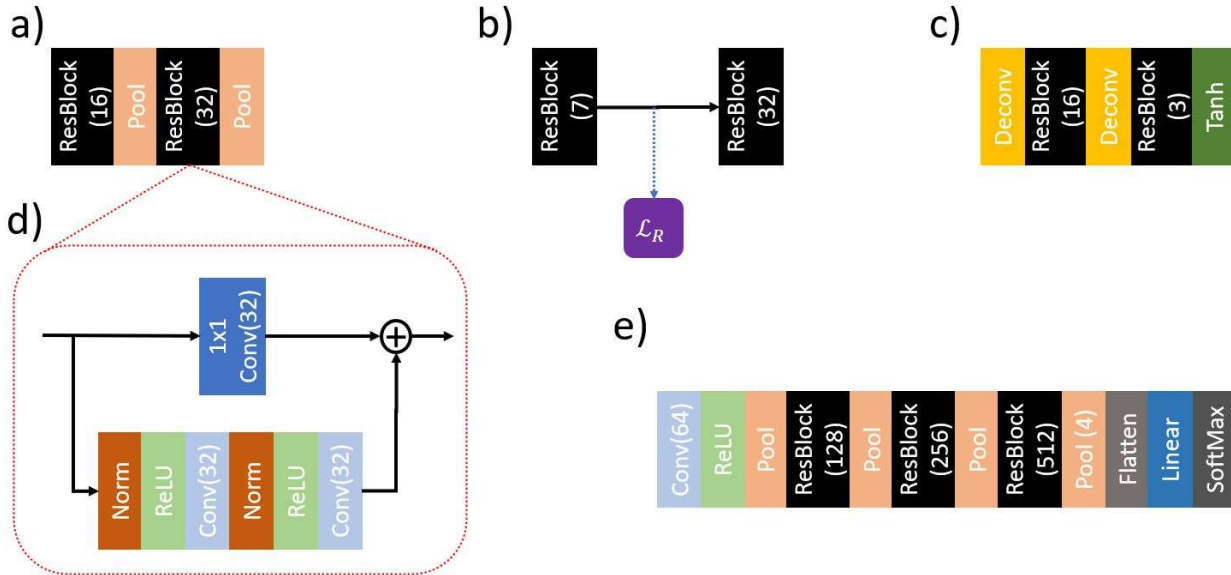


Figure 12: Architecture of a) encoder, b) bottleneck, c) decoder, and d) residual block, e) classifier used in the DNA experiments with the CIFAR-10 dataset. Conv(K): 3x3, 1-stride, zero-padded 2D convolutional layer with K output filters. Pool: 2x2 max pooling. Norm: Batch normalization layer. Deconv: 2x2 transpose convolution layer (number of input and output channels are equivalent). 1x1 Conv(K): 1x1 2D convolution with K output filters. Linear: Densely connected layer with size 10 output.